


## Article

# Characterization of the Airflow Distribution near a Circuit Breaker's Cu-Ag-Alloy Electrode Surface during and after Breakdown

Jixing Sun <sup>1,\*</sup> , Chenxi Shao <sup>1</sup>, Kun Zhang <sup>1</sup>, Jiyong Liu <sup>1,2</sup>, Shengchun Yan <sup>3</sup>, Yang Liu <sup>2</sup> and Yan Zhang <sup>2</sup>

<sup>1</sup> School of Electrical Engineering, Beijing Jiaotong University, Haidian District, Beijing 100044, China; 23126334@bjtu.edu.cn (C.S.); kzhang202202@163.com (K.Z.); 11110011@ceic.com (J.L.)

<sup>2</sup> State Energy Group Shuohuang Railway Company, Suning 062350, China; hv\_bjtu@163.com (Y.L.); 11095021@ceic.com (Y.Z.)

<sup>3</sup> National Energy Group Shuohuang Railway Development Research Institute, Beijing 100080, China; 11074772@ceic.com

\* Correspondence: sanyou345@163.com; Tel.: +86-15801067328

**Abstract:** Circuit breakers, affected by multiple lightning strikes after the breaker has been tripped, can break down again, which will reduce the life of the circuit breaker and threaten the stable operation of the power system. Aiming at this problem, this research obtained the temperature diffusion process of the inrush current process of the circuit breaker's opening and breaking, using the Schlieren technique combined with existing image recognition technology to obtain the temperature characteristics of the airflow in the air gap of the contact, as well as the characteristics of the flow of air itself. The results of the study show that the circuit breaker breakdown process generates a shock wave with a velocity approximately equal to the speed of sound under the same conditions. The maximum velocity of the airflow boundary diffusion is about one-quarter of the speed of sound under the same condition, and it decays very fast, reducing to the airflow drift velocity within 10 ms after breakdown. The maximum temperature of the thermals is concentrated between 6000 K and 8000 K, and the temperature change is approximately inversely proportional to the square of the time. This research provides the basis for the design of a circuit breaker's contact structure, opening speed optimization method, interrupter chamber, and insulation design optimization.

**Keywords:** gas-insulated; Schlieren method; plasma contact structure; breakdown airflow



**Citation:** Sun, J.; Shao, C.; Zhang, K.; Liu, J.; Yan, S.; Liu, Y.; Zhang, Y. Characterization of the Airflow Distribution near a Circuit Breaker's Cu-Ag-Alloy Electrode Surface during and after Breakdown. *Coatings* **2024**, *14*, 305. <https://doi.org/10.3390/coatings14030305>

Academic Editor: Giorgos Skordaris

Received: 31 December 2023

Revised: 20 February 2024

Accepted: 28 February 2024

Published: 29 February 2024



**Copyright:** © 2024 by the authors. Licensee MDPI, Basel, Switzerland. This article is an open access article distributed under the terms and conditions of the Creative Commons Attribution (CC BY) license (<https://creativecommons.org/licenses/by/4.0/>).

## 1. Introduction

Circuit breakers are important equipment for power system fault protection, which will disconnect the contacts and remove the affected line when they sense overvoltage, a high current during normal operation and fault [1–5]. According to the analysis of circuit breaker breakdown accidents caused by lightning strikes in many places, after experiencing a lightning-induced trip, if the circuit breaker undergoes a lightning strike again during hot standby reclosure [6–10], a wave will undergo total reflection at the gap break of the dynamic and static contacts, generating a doubling of the lightning overvoltage and superimposing it on the industrial frequency power transmission voltage [11–15], causing the overall overvoltage level to exceed the insulation level of the circuit breaker's opening gap, resulting in the breakdown of the circuit breaker's gap [16–20].

Different arc models during the breakdown process of circuit breakers have been proposed by Cassie A.M., Mayr O, L.S. Frost, and others [16–21]. Cassie suggests that the arc voltage remains approximately constant under high-voltage conditions, and the arc energy is proportional to the rate of change of the arc cross section. Mayr suggests that under low-current conditions, the arc is a cylinder with a constant diameter, and the dissipated power of the arc energy is approximately constant. L.S. Frost and others

consider the arc to be equivalent to a plasma generator, explaining that the sudden drop in arc conductivity during current zero-crossing is caused by the thermal diffusion of the arc.

Regarding the gas jet process during the operation of circuit breakers, relevant research has been conducted by Lin Xin [21], and others [22–24]. They found that intense turbulence is generated at the top of the electrodes during the arc burning process. Additionally, through simulation experiments on the structural model of the arc extinguishing chamber, they obtained data that are helpful for optimizing the design of circuit breaker arc extinguishing chambers [22–25].

Extensive research has been conducted by scientific research institutions such as the China Electric Power Research Institute, Beijing Jiaotong University, North China Electric Power University, and Shenyang University of Technology on the breakdown and recovery characteristics of insulation materials in circuit breakers [25–30]. The focus of the research has been the low-current cutoff of capacitor bank switches, the expected breaking characteristics of 10 kV rapid circuit breakers, and the pre-breakdown characteristics of 500 kV GIS circuit breakers. There is currently no publicly available information or theoretical research on insulation breakdown and the recovery processes between switch contacts under multiple lightning overvoltage conditions. Furthermore, there are no technical references or solutions available for the related engineering issues, highlighting the urgent need for further research in this area [31,32].

Extensive research has been conducted on the recovery process of circuit breaker insulation under the influence of multiple lightning strikes. The paper utilized the Schlieren method to capture the temperature diffusion process during the interruption of a circuit breaker's current. By combining existing image recognition technologies, the characteristic temperatures of the contact gap airflow and the flow patterns were obtained. These findings provide a basis for the design of circuit breaker contact structures, optimization methods for the interruption speed, and the optimization of arc extinguishing chambers and insulation design.

## 2. Thermal Diffusion Analysis of a Circuit Breaker's Breakdown Process

### 2.1. Electromagnetic Thermal Process Model

A circuit breaker's breakdown process is a multi-physical field coupling process; the process studied in this work includes the distribution of the thermal airflow process through three physical fields, electromagnetic–thermal, fluid heat transfer, and fluid flow, for the model building and initial boundary conditions. The first is the electromagnetic–thermal process, where all domains of the model satisfy the current conservation equations [32–34].

$$\nabla \cdot J = \rho V \quad (1)$$

$$J = \sigma E + \frac{\partial D}{\partial t} + J_E \quad (2)$$

$$E = -\nabla U, \quad (3)$$

where  $J$  is the current density, A/m<sup>2</sup>;  $\rho$  is the charge density, C/m<sup>3</sup>;  $V$  is the volume the charge occupied, m<sup>3</sup>;  $E$  is the electric field strength, V/m;  $D$  is the potential shift, C/m<sup>2</sup>; and  $U$  is the voltage, V.

The motion of the airflow field in the arc extinguishing chamber is more complex and is described and constrained here by the N-S equation, which includes the equations of mass conservation, momentum conservation, and energy conservation.

Mass conservation equation:

$$\frac{\partial \rho}{\partial t} + \frac{\partial \rho u}{\partial x} + \frac{\partial \rho v}{\partial y} + \frac{\rho v}{y} = 0 \quad (4)$$

Energy conservation equation:

$$\frac{\partial pe}{\partial t} + \frac{\partial pu(e+p/\rho)}{\partial x} + \frac{\partial pv(e+p/\rho)}{\partial y} + \frac{pv(e+p/\rho)}{y} = \frac{\partial(u\tau_{xx} + v\tau_{xy} + k\partial T/\partial x)}{\partial x} + \frac{\partial(u\tau_{xy} + v\tau_{yy} + k\partial T/\partial y)}{\partial y} + \frac{u\tau_{xy} + v\tau_{yy} + k\partial T/\partial y}{\partial y} + \rho V \quad (5)$$

The parameters considered during the analysis are as follows:  $\rho$  is the gas density,  $\text{kg}/\text{m}^3$ ;  $p$  is the gas pressure, Pa;  $x$  is the axial displacement, m;  $y$  is the radial displacement, m;  $u$  is the axial velocity, m/s;  $v$  is the radial velocity, m/s;  $Q$  is the arc source term, J;  $e$  is the unit internal energy, J;  $\tau$  is the viscous stress tensor;  $k$  is Boltzmann's constant,  $1.38 \times 10^{-23}$  J/K; and  $T$  is the temperature, K. Considering that the dynamic and static contacts are separated and the short electric arc between the contacts is a heat source, the non-isothermal flow equations corresponding to the fluid heat transfer module are set up as follows:

$$\rho C_p \frac{\partial T}{\partial t} + \rho C_p u \cdot \nabla T + \nabla \cdot q = Q + Q_p + Q_{vd} \quad (6)$$

$$q = -k \nabla T \quad (7)$$

$$\rho C_p \frac{\partial T}{\partial t} + \rho C_p u \cdot \nabla T + \nabla \cdot q = \nabla(k \nabla T) + Q \quad (8)$$

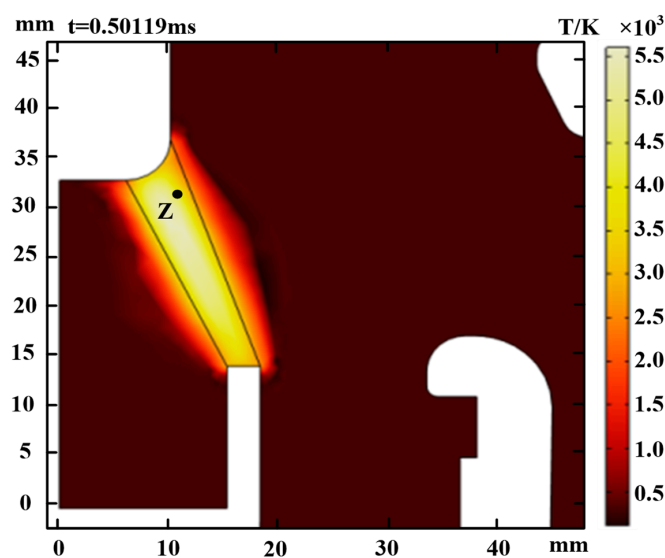
$$Q = \frac{\partial}{\partial T} \left( \frac{5k'T}{2q} \right) (\nabla T \cdot J) + E \cdot J + Q_{rad} \quad (9)$$

where  $C_p$  is the constant pressure heat capacity, J/(kg·K);  $Q_p$  is the heat source of warming, J;  $Q_{vd}$  is the heat source of loss, J;  $k_B$  is the solid thermal conductivity, W/(m·K); and  $Q_{rad}$  is the total volume radiation coefficient, W/m<sup>3</sup>.

## 2.2. Analysis of the Breakdown Thermal Diffusion Process

In the simulation experiments, we set the dynamic and static arc contact spacing to 14 mm and the SF6 gas pressure to 0.11 MPa, and we referred to 1.1 for the modified control equations and boundary conditions, to obtain the temperature of the interrupter chamber at different moments. The temperature distribution cloud diagram is shown in Figure 1a at 0.50119 ms and in Figure 1b at 50.119 s.

The velocity distribution cloud diagram was also obtained and is shown in Figure 2a at 0.1 ms and in Figure 2b at 150 ms.



(a)

Figure 1. Cont.

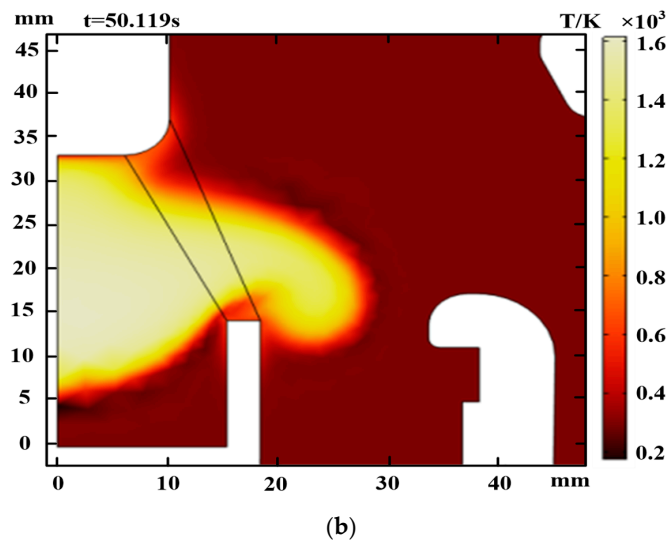


Figure 1. Airflow temperature distribution. (a) Cloud view of the initial moment of ignition; (b) Temperature distribution after 50 ms.

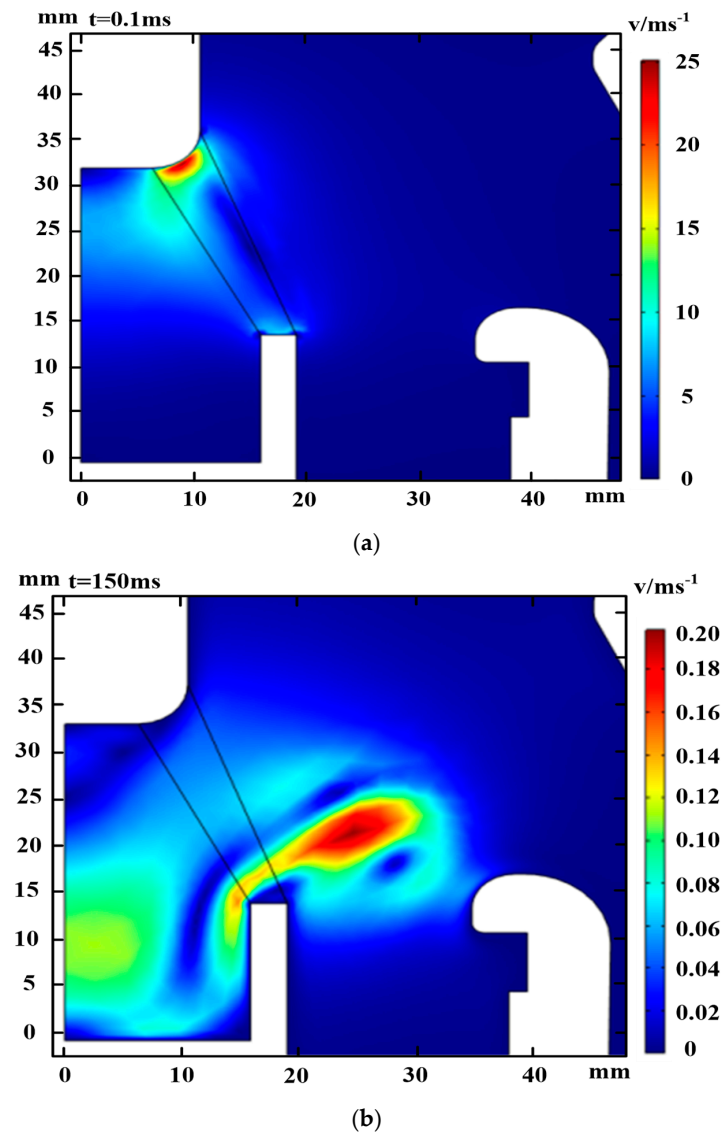


Figure 2. Airflow velocity distribution. (a) Initial velocity of the plasma; (b) Plasma velocity after 150 ms.

The temperature, motion speed, and conductivity characteristics of the thermal airflow at the typical position Z all reached the maximum value just after the discharge breakdown and decreased sharply after the end of the discharge. The rate of change of the characteristic quantities was fastest in the early stage of the breakdown and decreased gradually in the late stage of the breakdown, as shown in Figures 3–5.

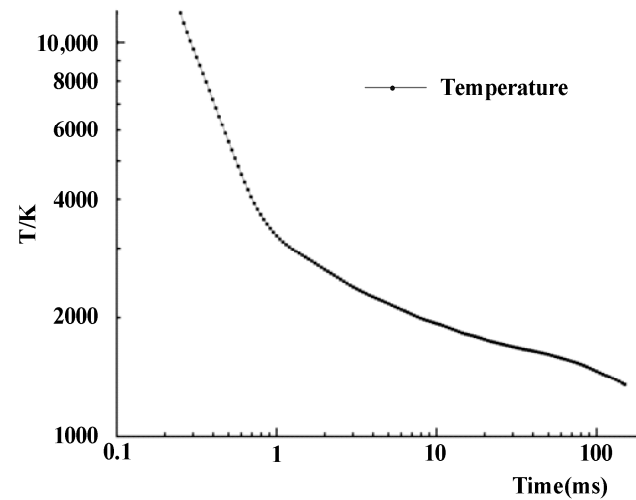


Figure 3. Temperature–time relationship.

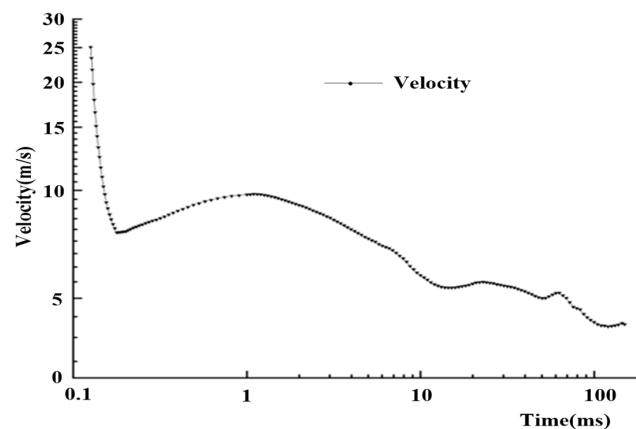


Figure 4. Velocity–time graph of the thermal airflow.

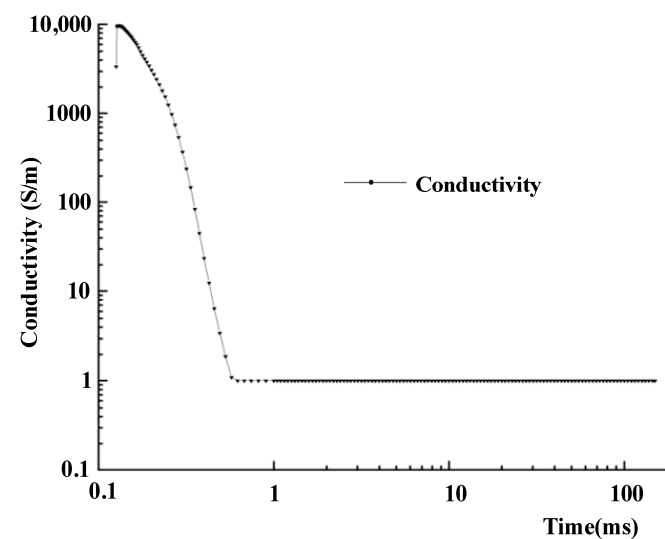
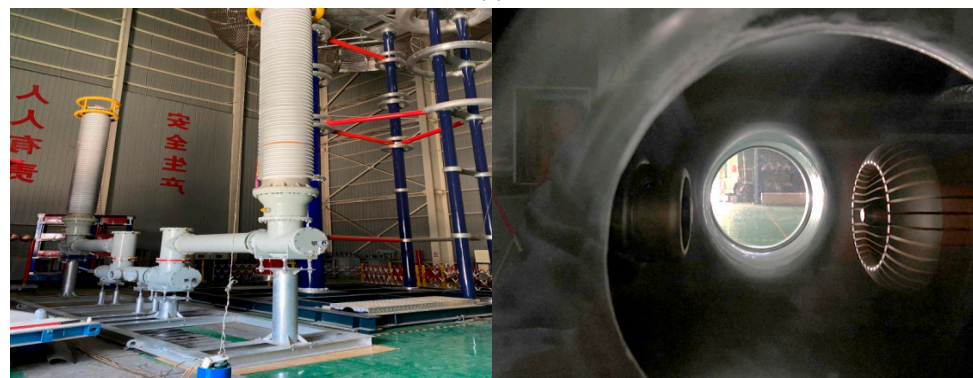
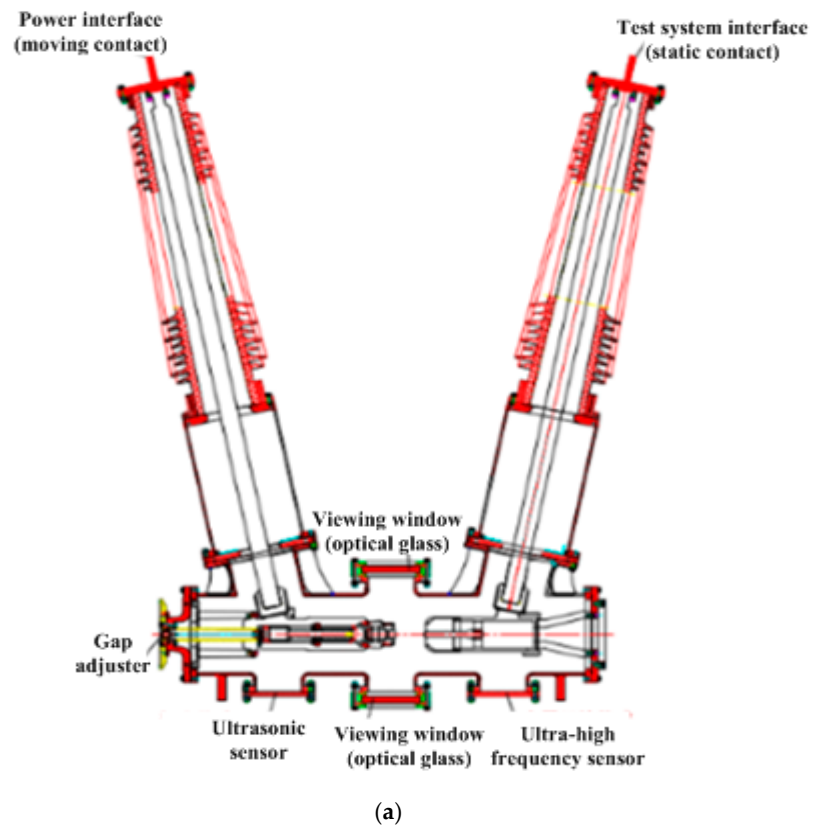


Figure 5. Conductivity–time relationship.

### 3. Breakdown Process and Thermal Process Test Research

#### 3.1. Experimental Procedure

The gas-insulated circuit breaker breakdown experimental platform mainly comprised three parts: an adjustable gap circuit breaker experimental device (shown in Figure 6), where both ends of the bushing can withstand high voltage, it has good external insulation, the lightning overvoltage generator can generate an impulse current of 35 kA, and it has a ripple image acquisition device (schematic diagram shown in Figure 7).



**Figure 6.** The test sample and the gap. (a) Test device diagram; (b) Test on field.

First, according to Table 1, we adjusted the contact spacing; second, the output current of the impact current generator was continuously adjusted to finally obtain the circuit breaker breakdown current under different air pressure conditions.



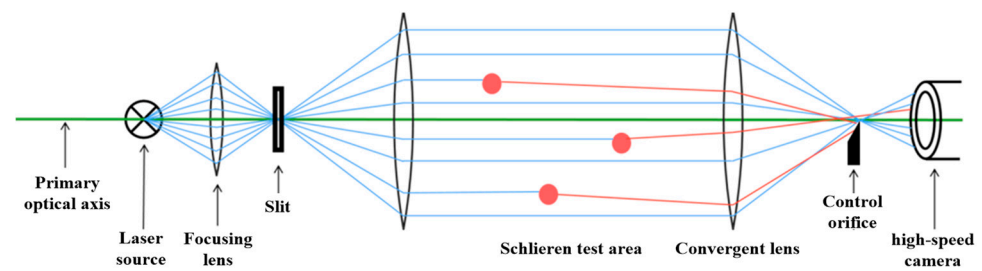


**Figure 7.** Working principle of Schlieren device.

**Table 1.** Test results of impulse voltage.

Arc Contact Spacing/cm	Breakdown Current/kA
0.6	10.357
0.8	12.092
0.9	13.857
1.0	13.861
1.2	15.452
1.4	16.632

### 3.2. Study on the Development Speed of the Thermal Air Flow

Analyzing the ripple images of the same air pressure with different electrode spacings, the approximate rectangular image in the center of each image showed the ripple outline of the moving contact, the trapezoidal bulge in the center of the right side of the moving contact was the ripple outline of the moving arc contact, and the space between the moving contact and the arc-shaped observation window on the right side of the image was the air gap for discharging; the moments of shooting in the demonstration pattern from left to right and from top to bottom were approximated to be exponential increments.

The pixel length occupied by the diameter of the moving arc contact in the grain image was about 679 pixels long, and the conversion ratio for one pixel point was 0.1296 mm to obtain the actual length.

$$d_0 = \frac{d_h}{N_0 \times N_h} = \frac{88}{1 \times 679} = 0.1296 \quad (10)$$

In the equation,  $d_0$  is the actual length represented by the unit pixel, mm;  $d_h$  is the actual length of the moving arc contact design, mm;  $N_0$  is the number of unit pixels; and  $N_h$  is the average pixel percentage of the moving arc contact.

Before the test, the slit and light path were adjusted, and the gray value obtained by the test was compared with the indoor temperature and the flame standard temperature. The breakdown process and Schlieren image data are shown in Figure 8, when the 20 kA current was applied. The speed of sound in the SF<sub>6</sub> gas was 135.38 m/s at 300 K, the pressure of the SF<sub>6</sub> gas was 0.11 MPa, and the propagation speed of the excitation wave within 1 ms after the discharge, measured at the above sampling point, was up to 141.35 m/s, which was about the same as the speed of sound in SF<sub>6</sub>.

### 3.3. Calculation of the Boundary Temperature of the Thermal Air Flow

Considering that the SF<sub>6</sub> thermal decomposition temperature is 774 K, the initial thermoelectric ionization temperature of gas is 3000 K, and the typical gas ionization temperature is 6000 K–8000 K, the extraction of the thermal airflow motion characteristics is mainly aimed at the thermal airflow in different frame rates under the characteristics of airflow boundary diffusion, locating different boundaries of the arc segment diffusion sampling analysis, as shown in Figure 9.

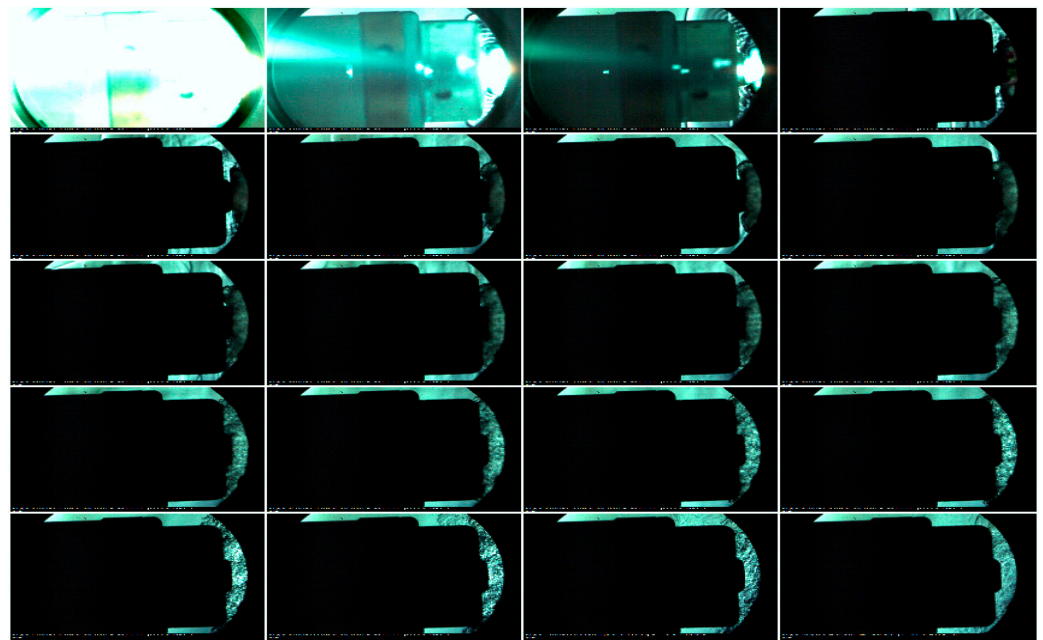


Figure 8. Sequential display of Schlieren image data.

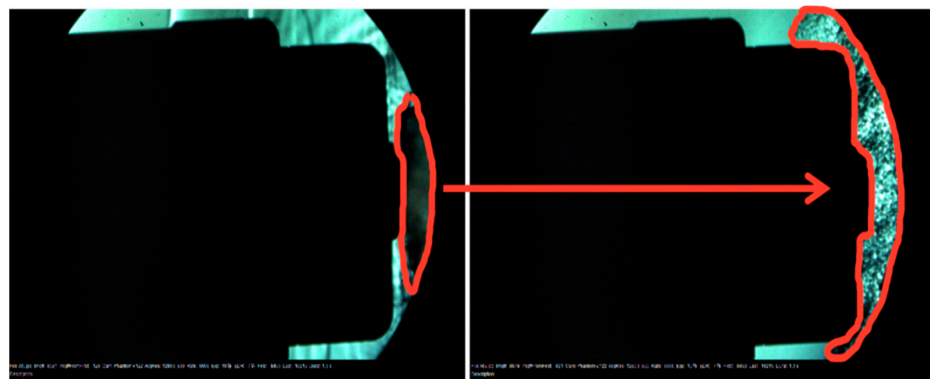


Figure 9. Thermal flow boundary diffusion.

MATLAB was used to convert the image data into grayscale matrix data, as shown in Figure 10, and the airflow motion boundaries were calibrated using the grayscale values corresponding to the unbroken image and the standard temperature values.

Based on this method, the hot gas stream boundary temperature development characteristics were obtained; the hot gas stream temperature reached 5000 K about 1 ms after the end of the discharge, and it was basically maintained below 1000 K and decreased at a relatively slow rate 10 ms after the end of the discharge, as shown in Figure 11. At the same time, it presented a similar oscillatory tendency with the movement of the hot gas stream on the logarithmic scale. The oscillatory period of the gas stream temperature was similar to that of the gas stream velocity on the logarithmic scale, but the amplitude of the data oscillations was much smaller, which was due to the fact that, compared to the mass inertia of the gas, the thermal inertia of the gas was much larger, and the damping of the temperature system was much larger than that of the motion system; therefore, the amplitude of the temperature characteristics of the oscillations was much lower.





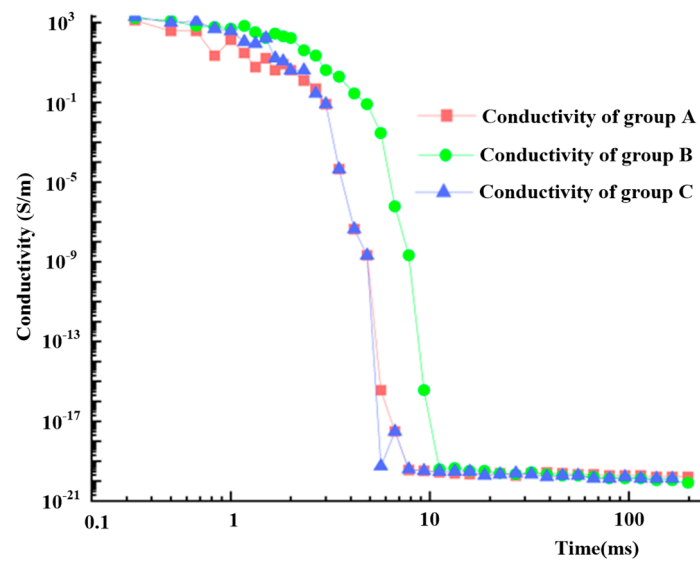


Figure 12. Conductance feature of the airflow.

#### 4. Conclusions

This work aimed at the problem of electrothermal re-breakdown during the opening process of a circuit breaker, studying the temperature diffusion process during the inrush current process of circuit breaker opening and breaking based on the Schlieren method and combining existing image recognition technology to obtain the temperature characteristics of the airflow in the air gap of the contacts, as well as the characteristics of the airflow itself. Specific conclusions were obtained as follows:

- (1) At the early stage of a circuit breaker's breakdown and discharge, the surge wave speed is maintained approximately at the speed of sound in the ambient condition, the movement speed of the hot airflow shows a decay characteristic, which is inversely proportional to the square of the time, the speed of the airflow at the observable initial moment is 34.33 m/s at the maximum, and the maximum airflow diffusion speed is 22.79 m/s at the electrode spacing of 1.0 cm.
- (2) The temperature of the hot gas stream is 8051 K at the end of the discharge process, and the maximum value of the gas stream diffusion velocity is 8051 K when the electrode spacing is 1.0 cm under the SF<sub>6</sub> gas pressure of 0.11 MPa. This will affect the electric field near the electrode surface, increasing the risk of impact penetration when overvoltage occurs.
- (3) The hot gas conductivity is affected by the plasmonization of the gas, and the insulating property of the gas is fully recovered when the temperature is lower than 3500 K, i.e., the electrical insulation strength of SF<sub>6</sub> is basically recovered about 10 ms after the end of the discharge, and the trend of recovery of the insulation strength of different groups tends to be the same. It is recommended to consider these data when designing breaker opening–closing speed and break spacing.

**Author Contributions:** Conceptualization, C.S.; Methodology, K.Z. and Y.L.; Software, C.S. and Y.L.; Investigation, J.S., K.Z., S.Y. and Y.Z.; Resources, J.S. and J.L.; Data curation, S.Y.; Writing—original draft, Y.Z.; Writing—review & editing, J.L. All authors have read and agreed to the published version of the manuscript.

**Funding:** This work was supported by the National Natural Science Foundation of China 52377131), Science and Technology Project of National Energy Group (SHTL-21-08, SHSN-22-05, SHTL-2022-9, SNFZ23086).

**Institutional Review Board Statement:** Not applicable.

**Informed Consent Statement:** Not applicable.

**Data Availability Statement:** Data are contained within the article.

**Acknowledgments:** The authors would like to thank the reviewers for their pertinent comments that help to improve the quality of this paper.

**Conflicts of Interest:** Jiyong Liu, Yang Liu and Yan Zhang were employed by the State Energy Group Shuohuang Railway Company. Shengchun Yan was employed by the State Energy Group Shuohuang Railway Development Research Institute. The remaining authors declare that the research was conducted in the absence of any commercial or financial relationships that could be construed as a potential conflict of interest.

## References

1. Khakpour, A.; Methling, R.; Gortschakow, S.; Uhrlandt, D.; Imani, M.T. An improved arc model for vacuum arc regarding anode spot modes. *IEEE Trans. Dielectr. Electr. Insul.* **2019**, *26*, 120–128. [[CrossRef](#)]
2. Smajkic, A.; Hadzovic, B.B.; Muratovic, M.; Kim, M.H.; Kapetanovic, M. Determination of Discharge Coefficients for Valves of High Voltage Circuit Breakers. *IEEE Trans. Power Deliv.* **2020**, *35*, 1278–1284. [[CrossRef](#)]
3. Terada, M.; Urai, H.; Yokomizu, Y. Method of Evaluating Exhaust Characteristics of High-Voltage Circuit Breaker. *IEEE Trans. Power Deliv.* **2020**, *35*, 707–714. [[CrossRef](#)]
4. Frost, L.S.; Liebermann, R.W. Composition and transport properties of SF 6 and their use in a simplified enthalpy flow arc model. *Proc. IEEE* **1971**, *59*, 474–485. [[CrossRef](#)]
5. Lowke, J.J.; Ludwig, H.C. A simple model for high-current arcs stabilized by forced convection. *J. Appl. Phys.* **1975**, *46*, 3352–3360. [[CrossRef](#)]
6. Swanson, B.W.; Roidt, R.M. Boundary layer analysis of an SF<sub>6</sub> circuit breaker arc. *IEEE Trans. Power Appar. Syst.* **1971**, *PAS-90*, 1086–1093. [[CrossRef](#)]
7. Wu, Y.; Wu, Y.; Rong, M.; Yang, F.; Zhong, J.; Li, M.; Hu, Y. A New Thomson Coil Actuator: Principle and Analysis. *IEEE Trans. Compon. Packag. Manuf. Technol.* **2015**, *5*, 1644–1655.
8. Hermann, W.; Kogelschatz, U.; Niemeyer, L.; Ragaller, K.; Schade, E. Experimental and theoretical study of a stationary high-current arc in a supersonic nozzle flow. *J. Phys. D Appl. Phys.* **2002**, *7*, 1703. [[CrossRef](#)]
9. Bort, L.S.; Franck, C.M. Effects of nozzle and contact geometry on arc voltage in gas circuit-breakers. In Proceedings of the IEEE International Conference on High Voltage Engineering & Application, Chengdu, China, 19–22 September 2016; IEEE: Piscataway, NJ, USA, 2016.
10. Ragaller, K.; Egli, W.; Brand, K.P. Dielectric recovery of an axially blown SF<sub>6</sub>-Arc after current zero: Part II-theoretical investigations. *IEEE Trans. Plasma Sci.* **1982**, *10*, 154–162. [[CrossRef](#)]
11. Sun, H.; Wu, Y.; Tanaka, Y.; Tomita, K.; Rong, M. Investigation on chemically non-equilibrium arc behaviors of different gas media during arc decay phase in a model circuit breaker. *J. Phys. D Appl. Phys.* **2019**, *52*, 075202. [[CrossRef](#)]
12. Mitchell, R.R.; Tuma, D.T.; Osterle, J.F. Transient Two-Dimensional Calculations of Properties of Forced Convection-Stabilized Electric Arcs. *IEEE Trans. Plasma Sci.* **1985**, *13*, 207–220. [[CrossRef](#)]
13. Inada, Y.; Matsumoto, H.; Matsuoka, S.; Kumada, A.; Ikeda, H.; Hidaka, K. Shack-Hartmann Type Laser Wavefront Sensor for Measuring Electron Density in Low Current Arc. *IEEE Trans. Fundam. Mater.* **2011**, *131*, 872–877. [[CrossRef](#)]
14. Trepanier, J.Y.; Zhang, X.D.; Pellegrin, H.; Camarero, R. Application of computational fluid dynamics tools to circuit-breaker flow analysis. *IEEE Trans. Power Deliv.* **1995**, *10*, 817–823. [[CrossRef](#)]
15. Zhang, J.M.; Yan, J.D.J. Effects of DC Component in Asymmetric Fault Current on the Thermal Recovery Characteristics of an SF<sub>6</sub> Autoexpansion Circuit Breaker. *IEEE Trans. Plasma Sci.* **2014**, *42*, 2117–2123. [[CrossRef](#)]
16. Karetta, F.; Lindmayer, M. Simulation of the gas dynamic and electromagnetic processes in low voltage switching arcs. *IEEE Trans. Compon. Pack. Technol. Manuf. Technol.* **1998**, *21*, 96–103.
17. Lindmayer, M.; Springstube, M. Three Dimensional Simulation of Arc Motion between Arc Runners Including the Influence of magnetic Material. *IEEE Trans. Compon. Pack. Technol.* **2002**, *25*, 409–414. [[CrossRef](#)]
18. Brown, B.R.; Mahajan, S.M. Circuit-Based Mathematical Model of an Arc Heater for Control System Development. *IEEE Access* **2021**, *9*, 143085–143092. [[CrossRef](#)]
19. Frost, L.S.; Lee, A. Interruption Capability of Gases and Gas Mixtures in a Puffer-Type Interrupter. *IEEE Trans. Plasma Sci.* **1980**, *8*, 362–367.
20. Robin-Jouan, P.; Yousfi, M. New Breakdown Electric Field Calculation for SF<sub>6</sub> High Voltage Circuit Breaker Applications. *Plasma Sci. Technol.* **2007**, *9*, 690. [[CrossRef](#)]
21. Fu, L.; Guan, Y.; Zhang, L.; Jin, H.; Wang, H.; Jing, Y. Study on the Mechanism and Influencing Factors of SF<sub>6</sub> Decomposition Products. *IOP Conf. Ser. Earth Environ. Sci.* **2021**, *657*, 012039. [[CrossRef](#)]
22. Lebouvier, A.; Delalondre, C.; Fresnet, F.; Boch, V.; Rohani, V.; Cauneau, F.; Fulcheri, L. Three-Dimensional Unsteady MHD Modeling of a Low-Current High-Voltage Nontransferred DC Plasma Torch Operating with Air. *IEEE Trans. Plasma Sci.* **2011**, *39*, 1889–1899. [[CrossRef](#)]
23. Song, Y.; Lin, X.; Zhou, T.; Wang, F. Simulation of Airflow Field and Breaking Capacity of 550 kV Fast Circuit Breaker. *High Volt. Eng.* **2023**, *49*, 2432–2441.

24. Zhang, Y.; Lü, Q.; Xiang, Z.; Guo, Z.; Li, X. Influence of Frequency on Arcing Characteristics of High-voltage Puffer SF6 Circuit Breaker. *High Volt. Eng.* **2023**, *44*, 3987–3994.
25. Toktaliev, P.D.; Semenev, P.A.; Moralev, I.A.; Kazanskii, P.N.; Bityrin, V.A.; Bocharov, A.N. Numerical modeling of electric arc motion in external constant magnetic field. *J. Phys. Conf. Ser.* **2020**, *1683*, 032009. [[CrossRef](#)]
26. Courant, R.; Friedrichs, K.; Lewy, H. On the Partial Difference Equations of Mathematical Physics. *IBM J. Res. Dev.* **1967**, *11*, 215–234. [[CrossRef](#)]
27. Xu, X.; Hu, W. Modeling and simulation of arc grounding fault of middle and low voltage distribution network based on ATP-EMTP. *J. Comput. Methods Sci. Eng.* **2020**, *20*, 1279–1288. [[CrossRef](#)]
28. Yuen, H.; Lax, M. Multiple-parameter quantum estimation and measurement of nonselfadjoint observables. *IEEE Trans. Inf. Theory* **1973**, *19*, 740–750. [[CrossRef](#)]
29. Katsunori, M.; Kenji, K.; Toshiro, S. Breakdown Effects of Dissolved SF6 Gas on Uniform Field in Perfluorocarbon Liquid. *IEEE Trans. Fundam. Mater.* **1999**, *119*, 311–316.
30. Roy, S.A.; Kiran, R.; Rao, M.M. Estimation of Gas Discharge Rates in EHV Gas Circuit Breakers. In Proceedings of the 2019 International Conference on High Voltage Engineering and Technology (ICHVET), Hyderabad, India, 7–8 February 2019.
31. Urai, H.; Koizumi, M.; Ooshita, Y.; Yaginuma, N.; Tsukushi, M. Measurement of hot gas exhaust characteristics in SF6 circuit breaker with small model interrupter. In Proceedings of the 2013 2nd International Conference on Electric Power Equipment-Switching Technology (ICEPE-ST), Matsue, Japan, 20–23 October 2013.
32. Yang, R.; Xu, M.; Yan, J.; Yang, M.; Geng, Y.; Liu, Z.; Wang, J. Decomposition Characteristics of SF6 under Arc Discharge and the Effects of Trace H<sub>2</sub>O, O<sub>2</sub>, and PTFE Vapour on Its By-Products. *Energies* **2021**, *14*, 414. [[CrossRef](#)]
33. Vajnar, V.; Vostracky, Z.; Sedlacek, J. Analysis of breaking capability within asymmetrical short circuits. In Proceedings of the 2015 16th International Scientific Conference on Electric Power Engineering (EPE), Kouty nad Desnou, Czech Republic, 20–22 May 2015.
34. Sun, J.; Song, S.; Li, X.; Lv, Y.; Ren, J.; Ding, F.; Guo, C. Restraining Surface Charge Accumulation and Enhancing Surface Flashover Voltage through Dielectric Coating. *Coatings* **2021**, *11*, 750. [[CrossRef](#)]

**Disclaimer/Publisher’s Note:** The statements, opinions and data contained in all publications are solely those of the individual author(s) and contributor(s) and not of MDPI and/or the editor(s). MDPI and/or the editor(s) disclaim responsibility for any injury to people or property resulting from any ideas, methods, instructions or products referred to in the content.